Physico-chemical study of an exogenic fulgurite from a thunderstorm on 10th August 2013 in Dallas, TX

Nuno M.S. Alte da Veiga[1], Francisco J. Martín-Gil[2], Jesús Martín-Gil[2], Elsa Maria Carvalho Gomes[1] and Pablo Martín-Ramos[3,*]

[1] Univ Coimbra, Centre for Earth and Space Research of the University of Coimbra, Department of Earth Sciences, Rua Sílvio Lima, 3030-790 Coimbra, Portugal. E-mail: ndaveiga@ci.uc.pt (NMSAV); egomes@dct.uc.pt (EMCG). ORCID: 0000-0001-6307-1859 (EMCG)

[2] Agriculture and Forestry Engineering Department, ETSIIAA, Universidad de Valladolid, Avenida de Madrid 44, 34004 Palencia, Spain. E-mail: montealeku@gmail.com (FJMG); mgil@iaf.uva.es (JMG). ORCID: 0000-0003-4989-6197 (FJMG); 0000-0001-9921-2465 (JMG)

[3] EPS, Instituto Universitario de Investigación en Ciencias Ambientales (IUCA), University of Zaragoza, Carretera de Cuarte, s/n, 22071 Huesca, Spain. Phone: +34 (974) 292668; Fax: +34 (974) 239302; E-mail: pmr@unizar.es. ORCID: 0000-0003-2713-2786.

Abstract

Droplet-like exogenic fulgurites comprise a minor grouplet of natural glasses resulting from powerful lightning strikes. Reports on such type-V fulgurites are scarce in the literature. In this work, a fulgurite specimen from the thunderstorm that took place on 10th August 2013, in Dallas, TX, USA, has been analyzed using X-ray powder diffraction, X-ray fluorescence, scanning electron microscopy, energy-dispersive X-ray spectroscopy, and infrared and Raman spectroscopy techniques. X-ray diffraction revealed the amorphous nature of the exofulgurite, and X-ray fluorescence showed a high Si, Al and Ca content. Infrared and Raman spectroscopy were key in revealing clear Si−O modes related signatures and a very significant presence of water (OH/H_2O). A parallel with glassy silicate materials, but also with opal-A, was essential in the understanding of the fulgurite's characteristics. In particular, Raman data evidenced the exofulgurite to have a high degree of depolymerization.

Keywords: droplet fulgurite; FTIR; keraunology; natural glass; Raman spectroscopy; telluric

1. Introduction

High-energy events, such as impact cratering (Chao 1967; Golubev et al. 2020; Koeberl and Ferrière 2019; Maierhofer et al. 2019), nuclear detonations (Eby et al. 2010; Roberts et al. 2019; Wannier et al. 2019), air bursts (Osinski et al. 2008; Silvia 2017; Wasson 2003) (Fig 1), or lightning strikes (Block 2011; Feng et al. 2019; Martín-Ramos et al. 2019; Roberts et al. 2019; Sheffer 2007; Stefano et al. 2020) produce materials that are geochemically and morphologically comparable. These materials include, for instance, aerodynamically-shaped teardrops, beads and dumbbell glasses; high-temperature rapidly quenched microspherules and vesicular siliceous scoria-like objects; corundum, mullite, magnesioferrite, suessite (Fe_3Si) or naquite (FeSi); and melted SiO_2 glass, or lechatelierite, which cannot be produced volcanically (Bunch et al. 2012).

Fulgurites are formed when a lightning strike, which generates temperatures of over 1,800 °C (3,270 °F), instantaneously melts silica, fusing grains together. A classification of fulgurites into four main types (Pasek et al. 2012; Pasek and Pasek 2018), considers as type I those fulgurites whose target material is typically an almost pure quartz sand (over 90%); type II fulgurites originate from loose sediments or soil with variable amounts of clay, silt, quartz sand and/or small rock fragments; type III are associated with caliche; whereas type IV fulgurites originate when lightning strikes hit directly rock outcrops (or at least, when target material clast size is larger than the diameter of the resulting fulgurite glass). A minor fifth type corresponds to droplet-like exogenic fulgurites; they are morphologically different from the previous ones and they originate in a very particular way. Conventional fulgurites are hollow glass tubes formed in the quartzose sand, soil or rocks hit by the lightning strikes. On the other hand, exogenic fulgurites (i.e., type V fulgurites), which are commonly associated with type II or type IV fulgurites, show a morphology that is consistent with ejection from the fulgurite cylinder or the top soil and a subsequent landing and cooling on the ground surface (eventually with significant cooling in the air). Visually, they are amorphous and often "bubbly" in appearance, show different colors (e.g., green) than those found in conventional fulgurites (which are typically tan or brown) and have a smooth, glassy surface (unlike conventional fulgurites which have a gritty, sandy feel) (Pasek et al. 2012).

The best documented cases of exogenic fulgurite occurrences took place in 2004 in Elko Hills, Northeastern Nevada, just south of the town of Elko (Mohling 2004) (Fig 2*a*), and in Oswego, NY, on 2nd August 2008 (Walter 2011) (Fig 2*b*). The total number of reported occurrences of this type of fulgurites is scarce, and even more when it comes to their study. Sometimes, the discovery of fulgurite specimens does not follow immediately the occurrence of a thunderstorm; this may cast an initial doubt on their origin, which may be particularly the case for type V droplet fulgurites. The case under study here took place during a strong thunderstorm on 10th August 2013, when a lightning bolt struck down a small tree in Mesquite, a suburban city located east of the city of Dallas, Texas. The next day, it was noticed that – apart from the charred remains of the tree – the ground was littered with bubbly, light and dark-green, “glass” pieces over a 4 m circular radius. The source of “glass emission” was traced to two small holes in the ground, from which molten liquid had apparently been shot up into the air in all directions. Specimens off the grass and nearby sidewalk were gathered before they were damaged by pedestrians and their discoverer began selling them online. The authors of this paper bought one of the specimens to study its composition (Fig 2*c,d*).

Even though several studies on fulgurites already exist, there is very limited data on the very particular case of exofulgurites, as previously mentioned, and questions arise about what type of geological object is created by a lightning strike in the particular circumstances of this one, and about the presence of singular features. Moreover, while several authors have already pointed to the importance of fulgurites’ investigation as a natural model for impact processes (Feng et al. 2019; Kochemasov 1985), the investigation of these natural glasses may have other relevant implications, namely as geological markers of paleoclimatic conditions (Carter et al. 2010a; Navarro-González et al. 2007; Pasek and Block 2009) and in telluric planetary studies. It is widely recognized that lightning strikes may have played an important role in Earth’s early stages, and the existence of lightning strikes has been recognized in Venus (Russell et al. 2007), and possibly in Titan (Petculescu and Kruse 2014). On other telluric planets, such as Mars, it is probable that at the time this planet had a thicker atmosphere, lightning strikes also occurred (Harrison et al. 2008). Fulgurites may thus be regarded as examples of such extreme environmental scenarios that need to be considered in a planetary geophysics context as well as in a terrestrial one.

2. Geological setting

The geology of Mesquite area, and in a broader way of Dallas County, is documented in general and more specific geological maps and memoirs on the region, including its soils (Barnes 1987; Coffee et al. 1980; Dallas Petroleum Geologists 1941; The University of Texas at Austin. Bureau of Economic Geology 1992; United States Geological Survey (USGS) 2014). The main geological unit in the area of Mesquite, and the one of interest herein, is the Ozan formation, which belongs to the Taylor Group (Late Cretaceous; Ku2 – Navarro and Taylor Groups, Fig 3). Navarro and Taylor groups strike regularly SSW-NNE for a few hundred kilometers, with an inflexion towards ENE in the extreme northeast of Texas. Ozan formation thickness shows values around 150 m in Dallas County; rocks from this unit dip eastwards at a very low angle (< 1º). Lithologically, Ozan formation consists of a medium to dark-gray calcareous clay, poorly bedded, with variable amounts of silt; silt content tends to increase upwards, with possible occurrence of fine-grained sand. Clay is montmorillonitic; some glauconite, phosphate pellets, hematite nodules and pyrite nodules are present. At surface, clayey soils, dark gray to black in the upper part (thickness in the range 40-120 cm) and dark gray to brown below, reflect the underlying lithology; total thickness may exceed 1.5 m.

3. Methods

The analytical approach to the study of the exogenic fulgurite sample included optical image and scanning electron microscopy (SEM) acquisition, as well as analyses by energy-dispersive X-ray spectroscopy (EDX), X-ray fluorescence spectroscopy (XRF), X-ray powder diffraction (XRPD), Fourier-transform infrared (FTIR) spectroscopy and Raman spectroscopy. In SEM acquisition, no sputter coating was used, in order to be able to perform EDX analyses. In the remaining analyses (XRF, XRPD, FTIR and Raman spectroscopy), the sample was ground into fine powder in an agate mortar, homogenized, and analyzed «as is».

Optical microscopy was undertaken with an Avangard Optics (China) AN-E500 iScope 500x USB digital microscope. SEM and EDX analyses were conducted with an EVO HD 25 (Carl Zeiss, Oberkochen, Germany) apparatus. Operative conditions are indicated in each SEM micrograph.

The elemental composition of the materials was determined by wavelength dispersive XRF spectroscopy with a Bruker S8 Tiger Series 2 apparatus, using the standardless analysis program QuantExpress to convert atoms of each element into oxides. Operative conditions: 60 kV Cu 200 µm LiF200 0.23º. For comparison purposes, the analysis was repeated at the Research Technical Services of Universidad de Alicante, with a PW 2400 (Philips, Amsterdam, Netherlands) automatic sequential wavelength dispersive X-ray fluorescence spectrometer. The results were processed with the analytical software package SuperQ. In both cases, measurements were taken over the homogenized sample powder, with at least 3 measurements per analysis.

The X-ray powder diffractogram of the sample was obtained using a Rigaku (Tokyo, Japan) D/max 2500 diffractometer, in reflection geometry, with a Cu$K\alpha$ (λ=1.54 Å) radiation and using crystalline silicon as a standard. Operative conditions: 40 kV, 30 mA; 2θ=5-80º; step=0.02º; t=1 s/step. The analysis was repeated at the facilities of the Universidad de Zaragoza with equal results.

The infrared spectra were collected using a Thermo Scientific (Waltham, MA, USA) Nicolet iS50 FTIR spectrometer, equipped with an in-built diamond attenuated total reflection (ATR) module. The spectra were collected in the 400-4000 cm^{-1} region at room temperature, with a 0.5 cm^{-1} spectral resolution; a total of 128 scans per spectrum were co-added. Ten spectra were collected from subsamples in powder form, with no significant differences observed between them.

The Raman spectra were acquired at room temperature in the 133-3820 cm^{-1} range at 1 cm^{-1} spectral resolution on a Jasco (Easton, MD, USA) NRS-5100 dispersive Raman system (532.11 nm laser line; 600 lines/mm dispersion grating; 50×1000 μm slit; rejection filter 532.0 nm; resolution 6.83 cm^{-1}, 3.60 cm^{-1}/pixel; objective lens MPLFLN 20×; laser power 1.0 mW; attenuator OD0.6; 4-stage Peltier cooled CCD (UV-NIR range, 1024 × 255 pixel)). This characterization was also conducted at the Research Technical Services of Universidad de Alicante. In total, three powdered subsamples were analyzed, each with a minimum of three collected spectra.

4. Results and discussion

4.1. *Optical examination and SEM analysis*

The droplet fulgurite specimen was light-green in color, and consisted of a main body, roughly spherical (diameter <1 cm), and minor spherical protuberances, some of them no bigger than 1-2 mm in diameter; the overall size was approximately 1.5 cm (Fig 2*c,d*). Optical microscope images (Fig 4) showed a material with glassy appearance, already observable in hand-specimen observation. Microscopic observation of some of the spherical protuberances revealed the presence of a very high number of light-halo vesicles; the existence of such vesicles was already observable macroscopically, some being bigger than 0.5 mm in diameter (Fig 2*d*). They are clearly indicative of the presence of rapid expanding volatiles leading to the formation of glass bubbles as a consequence of extreme heating associated to the lightning strike.

Scanning electron microscopy (SEM) micrographs of the surface of the microprotuberances (Fig 5) showed a body with a «crater-like» appearance, as it would be expected from above observations. The fulgurite appeared to be constituted by a groundmass with an amorphous appearance, with no visible individual mineral grains. It did not show the flow textures characteristic of lechatelierite formed at >2,200 ºC, such as those exhibited by the microspherules or SLOs from the Younger Dryas episode 12.9KYrBP (Fig 6). This feature indicates that, in the formation of the exofulgurite from Dallas, this temperature was not reached.

4.2. ***X-ray fluorescence and EDX studies***

The exofulgurite originates from soil material. The main soil constituents are also those present in the underlying calcareous montmorillonitic clay. The soil is smectitic and calcareous, the very high shrink-swell potential of the soil being strongly indicative that the smectite is a main constituent of the soil (Coffee et al. 1980; Templin et al. 1956). In this context, in a temperate climate with annual average precipitation over 900 mm, usual soil evolution leads to a loss of alkalis; particularly in what concerns CaO, a loss in the carbonate content leads to a residual enrichment in the smectitic and silt fractions in the soil, and consequently to an enrichment in silica content.

Chemical composition from XRF and EDX analyses is presented in Table 1. It reflects the montmorillonitic clayey nature of local lithology and its soil, namely for MgO content. The high CaO content is clearly related to the clay/soil being calcareous; K_2O can be linked to the occurrence of glauconite. The EDX analyses of the surface of one of the fulgurite's minor spherical protrusions indicated the existence of some local heterogeneity, the major difference being the absence of iron. Content of Fe_2O_3(total) for XRF results may be at least partially linked to the presence of iron-bearing nodules in the clay, which could account for an heterogeneous distribution of iron in the soil, and thus its absence in one minor protrusion. However, it is not clear that the nodules alone may account for Fe_2O_3(total), a fraction of this content being likely in connection with montmorillonite, marginally also with glauconite; as such, a local compositional fractionation related with the fulgurite formation process is likely to have occurred (this will be further discussed below).

XRF analytical results for the bulk sample (Dallas fulgurite), together with chemical composition data for other fulgurites, are presented in Table 2[i]. This table gathers examples of fulgurites of the same type as the Dallas fulgurite (i.e., type V), but also of type II and type IV specimens (the ones with which exogenic fulgurites are commonly associated). The specimens from York, Vernal and Tiedra are droplet-type fulgurites. York and Vernal samples are associated with type II fulgurites, the parent material being a mica-schist derived soil and a loess, respectively (Pasek et al. 2012); Tiedra specimens are related to an archaeological site (Martín-Ramos et al. 2019). The Greensboro fulgurite is a type II specimen originated from a red-brown clayey soil (formed from the weathering of a diabase) (Carter et al. 2010a). The Viseu (Abrunhosa et al. 1995) and Mottarone (Elmi et al. 2017) fulgurites are both type IV, associated with granites. The Zacatecas type II fulgurite was found in a calcareous soil (Reyes-Salas et al. 2017).

Chemical composition data in Table 2 reflect two major influences: origin and chemical composition fractionation during the rapid heating/fusion/solidification process associated with a lightning strike (which is recognized in a number of works, including some cited in Table 2). The Viseu fulgurite shows little compositional differences towards the parent granite, whereas the Mottarone fulgurite is clearly more silica rich than the granite it derives from. A similar process of silica enrichment is clear

---

[i] For additional XRF data from other type I, type II and type IV fulgurites, the interested reader is referred to the recent article by Roberts et al. (2019).

for the Greensboro diabase soil-related fulgurite. In the case of Zacatecas, the occurrence of a fractionation process is clear, with a silica-enriched and calcium depleted cover, and a high CaO content vitreous core. The same process of silica enrichment is present in the droplet-type fulgurites of Vernal and York, in respect to the type II fulgurites they are related with, along with an enrichment in K_2O and a loss in all other major element oxides (those with values above 1% in Table 2). The wide occurrence of compositional fractionation in fulgurites, including exogenic fulgurites, makes it very probable that the same process took place in the case of the Dallas fulgurite; fractionation has already been discussed in what concerns iron, but the same process is likely to be more widespread, namely in what concerns silica enrichment.

Fulgurites are usually considered as mineraloids. However, the fusion-solidification process involved in their formation has a parallel in some volcanic rock-types. With this in mind, and in order to compare the Dallas fulgurite composition with those of other fulgurites, CIPW norms (Cross et al. 1912) were calculated (see Table 2); they show a clear difference between normative corundum + hypersthene fulgurites and normative diopside + wollastonite + titanite fulgurites. The Dallas fulgurite belongs to this last group, together with Tiedra and the core Zacatecas fulgurite.

4.3. ***X-ray powder diffraction study***

The X-ray powder diffractogram (Fig 7) showed no peaks associated with the presence of crystalline phases. Therefore, it confirmed that the fulgurite specimen was entirely constituted by vitreous material.

The amorphous nature of the Dallas fulgurite prevented any quantitative identification of potential mineralogical components by XRPD, making it necessary to use complementary characterization techniques, namely FTIR and Raman spectroscopies.

Moreover, the extremely low number of reported occurrences of exogenic fulgurites, and even scarcer existence of corresponding analytical data, led us to look for a proxy. At this stage, emphasis was placed on the specimen composition and its crystallinity degree. Opal-A was chosen as a proxy, on the basis of its amorphous character, its siliceous composition and the presence of water (OH / H_2O), which was expected to be also present in the exofulgurite under study (and later on confirmed). Silica glass (in a broad sense) was used as another proxy.

The exofulgurite X-ray powder diffractogram showed a main broad asymmetric peak, very similar to data of several specimens of opal-A (Drees et al. 1989; Eckert et al. 2015; Liesegang and Milke 2014; Smith et al. 2018) and of silica glass (Gerber and Himmel 1986; Kivi et al. 2016; Wan et al. 2016; Warren and Loring 1935). However, there was a minor difference in the 2θ (Cu $K\alpha$) position of the diffuse peak: ~24.2º for the fulgurite versus ~22.2º for opal-A and ~21.3º for pure silica glass. In the latter case, for soda-lime-silica glass, the 2θ value increases to ~23.5º (12.4% CaO, 11.4% Na_2O, 76.3% SiO_2; (Biscoe et al. 1941)) and ~23.9º (8.1% CaO, 3.2% MgO, 13.2% Na_2O, 72.51% SiO_2; (Chakraborty et al. 2010)).

The fact that the fulgurite's diffractogram (total sample) shows that the specimen is entirely amorphous strongly supports the absence of soil/sand grains being embedded in the matrix. As such, either the exogenic fulgurite did solidify in the air or at least it had cooled down enough, when it hit the ground, not to embed soil particles in the matrix.

4.4. *FTIR spectroscopic studies*

For spectral interpretation and analysis, the infrared spectrum (Fig 8*a*) can be divided into two regions: 400 – 1500 cm^{-1}, comprising of a number of bands common to all silicates with tetrahedrally coordinated silicon (Farmer 1974; Graetsch et al. 1994; Langer and Floerke 1974; Plyusnina 1979; Webb and Finlayson 1987); and the second region, 1500 – 4000 cm^{-1}, which contains water-related (Efimov et al. 2003; Goryniuk et al. 2004) and organic matter-related C-H vibrational modes (Ganesh Kumar et al. 2014; Garai et al. 2006). The infrared spectrum of the Dallas fulgurite is characterized by three bands at 460, 784 and 1069 cm^{-1} attributed to a O-Si-O bending (δ(O-Si-O)), symmetric (ν_s(Si-O)) and asymmetric (ν_{as}(Si-O)) Si-O-Si stretching vibrations, respectively (Farmer 1974; Smallwood et al. 1997; Webb and Finlayson 1987). The peak positions of these bands compared to pure silica glass (Bock and Su 1970), opal-A (Gemological Institute of America 2020), and calcium aluminosilicate glass (70 mol% SiO_2, 10 mol% Al_2O_3, 20 mol% CaO; i.e., a composition similar to that of the Dallas fulgurite) (Huang and Behrman 1991) are found in Table 3. The positions of the characteristic vibrational modes of opal-A and the calcium aluminosilicate glass are very similar to those of the Dallas fulgurite.

Figure 8 presents an infrared spectrum of the Dallas fulgurite (solid line) together with the infrared spectra of quartz (black dotted line) and opal-A (red dotted line) for visual comparison. Of particular note is the ν_{as}(Si-O) band at 1069 cm^{-1} which is significantly broader in the spectrum of the Dallas fulgurite compared to quartz and opal-A, a feature that is usually associated with amorphous materials. Additional spectral features, which appear as distinctive shoulders at ~965 and ~1175 cm^{-1}, contribute to broaden this band. A similar pattern is observed in the infrared spectrum of calcium aluminosilicate glass with the band in the 1050–1100 cm^{-1} region and the band at ~960 cm^{-1} assigned to the stretching vibration of the Si–O bond of the [SiO_4]

tetrahedra, with one corner shared with an aluminum or calcium polyhedron (Si(OA1/Ca) group) in the first case, or with two corners shared with aluminum-oxygen or calcium-oxygen polyhedra ($Si(OA1/Ca)_2$ group) in the second case (Huang and Behrman 1991). The number of non-bridging oxygens increases with excess CaO, these “modifiers” breaking the inter-tetrahedral bonds, a phenomenon also referred to as “depolymerization” of the glassy network (Khalil et al. 2010). In addition, the position of the ν_{as}(Si–O) band at ~1100 cm^{-1} is an indicator of the three-dimensionality of the silica network, a shift towards lower wavenumbers indicating that the network is weaker or in lower three-dimensionality than fused pure silica glass (Kamiya et al. 2000). The band at ~1175 cm^{-1}, responsible for a shoulder in the main 1069 cm^{-1} band, may also be attributed to ν_{as}(Si–O) (Anbalagan et al. 2010).

According to Drees et al. (1989), the intensity of the 965 cm^{-1} band decreases from opal-A to more crystalline silica polymorphs, such as opal-CT and quartz. In the spectrum of opal-A, the band is due to ν(Si-O) of Si-OH groups (Hiro and Sato 1971), and the band intensity weakens as the Si-OH groups condense to form Si-O-Si bonds (Moenke 1974). In Fig 8a,*b*, this band in the opal-A specimen is visible in the spectrum as an inflexion superposed on the lower side of the main band. A similar Si-OH band, ~965 cm^{-1}, is also observed in water-containing amorphous silica, as silica gel, which may remain (although subdued) even when the sample is heated to relatively high temperatures (up to 400 ºC, or – depending on the cases – even 800 – 1000 ºC) (Huffman and McMillan 1985; Perry et al. 1991; Uchino et al. 1991).

Both the calcium and water content of the Dallas fulgurite may contribute to the spectral features observed in the 400-1500 cm^{-1} region.

A broad band is centered at ~3400 cm^{-1} in the fulgurite spectrum and, together with features at 2000, 1880 and 1631 cm^{-1}, indicates the presence of OH groups and/or bound H_2O (see Table 3 for specific band assignments).

The bands at 2358, 2855, 2926 and 2961 cm^{-1} (Fig 8*a,c*; Table 3) are due to C-H stretching vibrations (Ganesh Kumar et al. 2014; Garai et al. 2006), which indicates the presence of organic matter.

4.5. *Raman spectroscopic studies*

The Dallas fulgurite Raman spectrum (Fig 9), in the region up to 1250 cm^{-1}, is dominated by two broad bands, centered at ~480 and 1014 cm^{-1}, typical of glassy silicate materials. The intense band at ~480 cm^{-1}, with the presence of additional weaker bands, is assigned to the twisting (τ(Si–O–Si)) and bending (δ(Si–O–Si)) modes of the SiO_4 tetrahedral units. Bands in the high wavenumber region – 800 and 1014 cm^{-1} – are associated with ν_s(Si-O) of silica tetrahedra with one to four non-bridging oxygen atoms (Carter et al. 2010a; Colomban and Slodczyk 2009; White and Minser 1984). Figure 9 presents the Raman spectra of the fulgurite together with the RRUFF database spectra of quartz and opal-A. The width of the ~480 cm^{-1} band is broader in the fulgurite spectrum than the corresponding band in the spectrum of quartz and opal-A, indicating that the fulgurite has a markedly amorphous character. The fulgurite's chemical analyses showed that its composition was mainly silica with high Al_2O_3 and CaO content, which is likely linked to the presence of the two strong broad bands observable in the fulgurite's Raman spectrum.

The Raman spectrum of the fulgurite in the spectral range 300-1250 cm^{-1} resembles results collected from a Ca-based glaze reported by Colomban (2005). In this work, within the high wavenumber region, spectral deconvolution revealed four bands corresponding to four, three, two, one/zero non-bridging oxygen atoms per silica tetrahedra, at increasing Raman shift values. The position of the band attributed to the four non-bridging oxygen atoms was observed in the range of ~800-850 cm^{-1}, similar to the position of the band at ~800 cm^{-1} in the fulgurite spectrum. Colomban (2005) measured the degree of polymerization by calculating the ratio of the area of the Si-O bending modes to the area of the Si-O stretching modes ($I_p = A_{500}/A_{1000}$). For the Dallas fulgurite this value was $I_p = 1.12$, which is outside the 1.3–2.5 interval defined for Ca glasses (Colomban and Slodczyk 2009) (the implications of these results will be discussed in section 5).

Further insight on the Raman data of the Dallas fulgurite can be achieved by comparing results with data from an investigation of White and Minser (1984) on natural glasses, which includes experimental work on synthetic glasses. An increasing Na_2O+Al_2O_3 (1:1) to SiO_2 ratio in soda-alumina-silica glasses was noted to influence the Raman spectrum, with the maximum of the mid-wavenumber region intense band shifting closer to 500 cm^{-1} (from 470 → 489 cm^{-1}); and two broad bands at 995 and 1095 cm^{-1} merging into a single band centered at 998 cm^{-1}. The Raman spectrum of the Dallas fulgurite is quite similar to the Raman spectrum collected from synthetic glass with the highest Na_2O+Al_2O_3 (1:1) to SiO_2 ratio. Similar to what happens in the side-area context of igneous rocks, aluminum would contribute to polymerize three-dimensional frameworks within the glass. On the other hand, alkali ions would depolymerize the three-dimensional framework with the creation of non-bridging oxygen atoms. Alkaline-earth ions would have a similar effect to the alkali ones; additionally, when their content is high, they would originate phase separation into silica-rich and silica-poor regions, with less and more than the expected number of non-bridging oxygen atoms, respectively. For this reason, silica-poor regions would have a high contribution to the observed spectra (White and Minser 1984; Winter 2010).

The Raman spectra of tektites and obsidians in White and Minser (1984)'s study show similar lineshapes in the 300-1250 cm^{-1} region, with two broad bands at ~437-467 and ~990-1151 cm^{-1}, and a band of low intensity at ~800 cm^{-1}, which is also the pattern observed for the Raman spectrum collected from the Dallas fulgurite. However, unlike the latter, along with a high intensity mid-wavenumber band, they all show a rather low intensity high wavenumber band, thus indicating a highly polymerized three-dimensional framework structure. Two particular samples may be highlighted: an Apollo 16 lunar glass (with a 42.7% silica; high Fe, Mg and Ca; and low alkalis content) and a synthetic «basalt» glass without iron; both show a band at ~1000 cm^{-1} stronger than the one at ~500 cm^{-1}, indicative of a high depolymerization degree. The Dallas fulgurite is intermediate between the two groups, closer to the latter than to the former, with a broad strong band at ~1014 cm^{-1}, albeit not as intense as the band at ~480 cm^{-1}. White and Minser (1984)'s NBO/T (non-bridging oxygen to bulk composition) index for the fulgurite shows a value between 0.27 (considering all Fe as Fe_2O_3), 0.32 (1:1) and 0.37 (considering all Fe as FeO) (0.02-0.07 for the tektites and obsidians, a maximum of 0.62 for the lunar glass and 0.74 for the «basalt»).

The fulgurite's Raman spectrum in the 1250-4000 cm^{-1} region (Fig 9*a*) is dominated by a massif with a double maximum at ~2060 cm^{-1} and ~3080 cm^{-1}, which likely includes weaker bands. In this region, it closely resembles the spectrum of an amorphous specimen of opal-A, as shown in Ostrooumov et al. (1999). A band at 1680 cm^{-1} (not evident in the fulgurite's rising curve) is associated with H-O-H vibration (McMillan and Remmele 1986), and the band at 3080 cm^{-1} is typical of molecular H_2O groups (Walrafen 1964).

5. Overall discussion

The Dallas exofulgurite chemical composition, see Table 1 and Table 2, indicates that it belongs to a specific group with normative diopside + wollastonite + titanite. Its high CaO content, together with silica and alumina, proved to have a role in its properties. XRPD confirmed its amorphous character, but delivered little more information. FTIR and Raman spectra were key in understanding the fulgurite's characteristics. The use of opal-A and silica glass (in a broad sense) as proxies, for which a wider amount of data is available, proved to be the second key in the study of the Dallas exofulgurite.

The FTIR spectrum revealed characteristic bands in the higher wavenumber region attributed to OH and/or H_2O-related modes and in the lower wavenumber regions bands related to Si-O bending and stretching vibration modes in silica tetrahedra. The band at 965 cm^{-1} (ν(Si-O) of isolated Si-OH groups), characteristic of lower crystallinity degree silica polymorphs, was more intense in the Dallas fulgurite than in the opal-A specimen in Fig 8, as well as in other cases in the literature; this 965 cm^{-1} band is present as a shoulder on the main 1069 cm^{-1} band, both reflecting the significant calcium content of the specimen. Thus, the shoulder at 965 cm^{-1} very likely corresponds to the superposition effect of Ca content and the presence of Si-OH groups. The overall indications from the FTIR spectrum were in the direction of the existence of some short-range silica tetrahedra structuration with relevant depolymerization, and the presence of water (OH / H_2O), possibly in significant amounts.

The exofulgurite Raman spectrum contained bands within two distinct regions: from 100 cm^{-1} to 1250 cm^{-1} and from 1250 cm^{-1} to 4000 cm^{-1}. The two strong broad bands centered ~480 cm^{-1} and ~1014 cm^{-1} are characteristic of glassy silicate materials, and are followed by a very broad high-intensity double maximum OH / H_2O related massif. Raman spectra results for opals show that an increase in the structural disorder in opals is accompanied by a broadening and reduction of the number of bands, and a considerable increase in the intensity and width of OH and H_2O related bands (Ostrooumov et al. 1999). By opal standards, the Raman spectrum of the exofulgurite in Fig 9 was indicative of a highly disordered material.

The fundamental factor was the possibility to evaluate the exofulgurite's depolymerization degree, from Raman data, on the basis that the Si-O bending/stretching modes are separately associated with the ~480 cm^{-1}/~1014 cm^{-1} massifs, the latter being related to the presence of non-bridging oxygen atoms in a material structure. The NBO/T index value for the fulgurite is in the range 0.27 to 0.37 (the role of iron being unclear); in any case significantly above values for tektites and obsidians (0.02 to 0.07), a higher value indicating higher depolymerization. Additionally, the I_p index value is low ($I_p = 1.12$), below the 1.3 lower limit defined for Ca glasses (a lower value indicating higher depolymerization). The NBO/T index is set on the basis of the mole content for major component oxides; the I_p index is calculated by determining the ratio of the areas under the ~500 cm^{-1}/~1000 cm^{-1} bands. Moreover, data from the fulgurite's FTIR and Raman spectra between 1250 and 4000 cm^{-1} revealed the existence of an important water (OH/H_2O) content (by opal standards). Strong indications in this direction came also from the highly vesicular character of the fulgurite's sample, as revealed by hand-specimen and optical microscope observation, as well as SEM images, indicative of an important volatile phase, and entirely compatible with a high water content near the soil surface during a thunderstorm.

OH groups and molecular water have a depolymerization effect that is not taken into account in the NBO/T index. The 1014 cm^{-1} massif in Raman spectra is partly due to the high CaO fulgurite's content; but a strong contribution most likely comes from OH groups and molecular water content. This would also explain the low I_p index value, below the 1.3-2.5 interval for Ca glasses. And, if the water effect was taken into account, the exofulgurite's NBO/T index should be higher, closer to the lunar Apollo 16 sample maximum value of 0.62.

In the broader context of telluric planets, depolymerization of the silicate melts could also result from the solution of methane, associated with the formation of OH-groups, or from the solution of carbon monoxide (Eggler and Baker 1982; Mysen and Richet 2005; Taylor 1987). As an example, this could be interesting in the case of Titan, in which there would possibly be lightning strikes in combination with CH_4, both as gas in the atmosphere and in liquid form on the surface (Hörst 2017).

Some weak peaks in the exofulgurite's FTIR spectrum are indicative of the presence of C-H bonds. The presence of carbon compounds in the sample is not unlikely, owing to the presence of organic matter in the soil from which the exofulgurite originated. In this respect, the presence of organic matter in fulgurites has also been reported by Elmi et al. (2017), who found bands suggestive of polyaromatic hydrocarbon molecules (cyclic alkenes) in the Raman spectra of the rock fulgurites from Mt. Mottarone (Piedmont, Italy), and by Carter et al. (2010b), who found polyaromatic hydrocarbons in a type-II fulgurite found in Greensboro (NC, USA).

A precise temperature value determination for the exofulgurite's formation is not possible. However, it can be constrained. The absence of flow textures, characteristic of lechatelierite formed at temperatures >2,200 °C, is indicative that this temperature was not reached. In fact, the I_p index value of 1.12 suggests much lower temperatures. Colomban (2005) indicates values of ca. 1,400 °C for $I_p \sim 7$; 1,000 °C for $I_p \sim 1$; and ca. 600 °C or less for $I_p \sim 0.3$. Experimental petrology data for a dacite-like composition (which is not very far from the fulgurite's chemical composition) points towards a dry solidus and liquidus temperature at surface pressure of 970 °C and 1020 °C, respectively (Gill 2010). On the basis of all these values, a temperature formation of ca. 1,000 °C, or lower, is likely for the exofulgurite (which applies particularly to solidification temperature). In this respect, a high water content contributes to lowering the fusion/solidification temperature of the material.

6. Conclusion

Fulgurites are formed under very particular circumstances, and the droplet-type Dallas exofulgurite originated in an even more particular way. Its mode of occurrence indicates that the fused target soil hit by the lightning strike was projected upwards into the air. The joint features of lightning strike origin, with an extremely rapid heating/fusion/solidification process, plus the exofulgurite's chemical composition (especially its CaO content), the high water content and – in particular – the high depolymerization degree of its structure make it unique. This last singular feature represents a clear difference in comparison with terrestrial tektites and obsidians. While, at this stage, a possible role of this high depolymerization degree of the fused silicate remains uncertain, the study of these natural glasses may serve as an analogue for telluric planetary studies in extreme environmental scenarios involving water, methane or carbon monoxide.

Acknowledgements

Mr. William T. Walker is gratefully acknowledged for kindly providing first-hand information on the impact site.

Conflict of interest statement

The authors declare no conflict of interest.

References

Abrunhosa M, Gonçalves AAHB, Cruz D (1995) Ocorrência de rochas vitrificadas no Dólmen do "Picoto do Vasco" (Vila Nova de Paiva, Viseu) Estudos Pré-históricos 3:167-185

Adamo I, Ghisoli C, Caucia F (2010) A contribution to the study of FTIR spectra of opals Neues Jahrbuch für Mineralogie - Abhandlungen 187:63-68 doi:10.1127/0077-7757/2010/0161

Aines RD, Rossman GR (1984) Water in minerals? A peak in the infrared Journal of Geophysical Research: Solid Earth 89:4059-4071 doi:10.1029/JB089iB06p04059

Anbalagan G, Prabakaran AR, Gunasekaran S (2010) Spectroscopic characterization of indian standard sand J Appl Spectrosc 77:86-94 doi:10.1007/s10812-010-9297-5

Barnes VE (1987) Geologic atlas of Texas, Dallas sheet (revised 1987). University of Texas at Austin, Bureau of Economic Geology, Austin, TX, USA

Biscoe J, Druesne MAA, Warren BE (1941) X-Ray Study of Potash-Silica Glass* J Am Ceram Soc 24:100-102 doi:10.1111/j.1151-2916.1941.tb14830.x

Block K (2011) Fulgurite classification, petrology, and implications for planetary processes. The University of Arizona

Bock JAN, Su G-J (1970) Interpretation of the Infrared Spectra of Fused Silica J Am Ceram Soc 53:69-73 doi:10.1111/j.1151-2916.1970.tb12012.x

Bunch TE et al. (2012) Very high-temperature impact melt products as evidence for cosmic airbursts and impacts 12,900 years ago Proc Natl Acad Sci 109:E1903-E1912 doi:10.1073/pnas.1204453109

Carter EA, Hargreaves MD, Kee TP, Pasek MA, Edwards HGM (2010a) A Raman spectroscopic study of a fulgurite Philos Trans Royal Soc A 368:3087-3097 doi:10.1098/rsta.2010.0022

Carter EA, Pasek MA, Smith T, Kee TP, Hines P, Edwards HGM (2010b) Rapid Raman mapping of a fulgurite Anal Bioanal Chem 397:2647-2658 doi:10.1007/s00216-010-3593-z

Chakraborty R, Dey A, Mukhopadhyay AK (2010) Loading Rate Effect on Nanohardness of Soda-Lime-Silica Glass Metallurgical and Materials Transactions A 41:1301-1312 doi:10.1007/s11661-010-0176-8

Chao ECT (1967) Shock effects in certain rock-forming minerals Science 156:192-202 doi:10.1126/science.156.3772.192

Coffee DR, Hill RH, Ressel D (1980) Soil survey of Dallas County, Texas.

Colomban P (2005) Case study: Glasses, glazes and ceramics—Recognition of ancient technology from the Raman spectra. In: Edwards HGM, Chalmers JM (eds) Raman spectroscopy in Archaeology and Art History. Royal Society of Chemistry, Cambridge, pp 192-206

Colomban P, Slodczyk A (2009) Raman intensity: An important tool to study the structure and phase transitions of amorphous/crystalline materials Opt Mater 31:1759-1763

Cross W, Iddings JP, Pirsson LV, Washington HS (1912) Modifications of the "Quantitative System of Classification of Igneous Rocks" The Journal of Geology 20:550-561

Dallas Petroleum Geologists (1941) Geology of Dallas County, Texas. Southern Methodist University, Dallas, TX, USA

Drees RL, Wilding LP, Smeck NE, Senkayi AL (1989) Silica in soils: Quartz and disordered silica polymorphs. In: Dixon JB, Weed SB (eds) Minerals in Soil Environments, vol 1. SSSA Book Series. pp 913-974. doi:10.2136/sssabookser1.2ed.c19

Eby N, Hermes R, Charnley N, Smoliga JA (2010) Trinitite-the atomic rock Geology Today 26:180-185 doi:10.1111/j.1365-2451.2010.00767.x

Eckert J et al. (2015) Ordering of water in opals with different microstructures Eur J Mineral 27:203-213 doi:10.1127/ejm/2015/0027-2428

Efimov AM, Pogareva VG, Shashkin AV (2003) Water-related bands in the IR absorption spectra of silicate glasses Journal of Non-Crystalline Solids 332:93-114 doi:10.1016/j.jnoncrysol.2003.09.020

Eggler D, Baker D (1982) Reduced volatiles in the system COH: implications to mantle melting, fluid formation, and diamond genesis Adv Earth Planet Sci 12:237-250

Elmi C, Chen J, Goldsby D, Gieré R (2017) Mineralogical and compositional features of rock fulgurites: A record of lightning effects on granite Am Mineral 102:1470-1481 doi:10.2138/am-2017-5971

Farmer VC (1974) The Infrared spectra of minerals. Mineralogical Society monograph, vol 4. Mineralogical Society, London

Feng T, Lang C, Pasek MA (2019) The origin of blue coloration in a fulgurite from Marquette, Michigan Lithos 342-343:288-294 doi:10.1016/j.lithos.2019.06.003

Ganesh Kumar A, Vijayakumar L, Joshi G, Magesh Peter D, Dharani G, Kirubagaran R (2014) Biodegradation of complex hydrocarbons in spent engine oil by novel bacterial consortium isolated from deep sea sediment Bioresour Technol 170:556-564 doi:10.1016/j.biortech.2014.08.008

Garai J, Haggerty SE, Rekhi S, Chance M (2006) Infrared Absorption Investigations Confirm the Extraterrestrial Origin of Carbonado Diamonds The Astrophysical Journal 653:L153-L156 doi:10.1086/510451

Gemological Institute of America (2020) Opal R060653. RRUFF Project. https://rruff.info/R060653. Accessed 18 December 2020

Gerber T, Himmel B (1986) The structure of silica glass Journal of Non-Crystalline Solids 83:324-334 doi:10.1016/0022-3093(86)90245-0

Gill R (2010) Igneous rocks and processes : a practical guide. Wiley-Blackwell, Chichester, West Sussex, UK ; Hoboken, NJ

Golubev YA, Shumilova TG, Isaenko SI, Radaev VA, Utkin AA, Makeev BA, Ernstson K (2020) Microscopic studies of ultra-high pressure glasses from impactites of the Kara astrobleme Journal of Non-Crystalline Solids 534 doi:10.1016/j.jnoncrysol.2020.119951

Goryniuk MC, Rivard BA, Jones B (2004) The reflectance spectra of opal-A (0.5–25 μm) from the Taupo Volcanic Zone: Spectra that may identify hydrothermal systems on planetary surfaces Geophys Res Lett 31 doi:10.1029/2004gl021481

Graetsch H, Gies H, Topalović I (1994) NMR, XRD and IR study on microcrystalline opals Phys Chem Miner 21:166-175 doi:10.1007/bf00203147

Harrison RG, Aplin KL, Leblanc F, Yair Y (2008) Planetary Atmospheric Electricity Space Science Reviews 137:5-10 doi:10.1007/s11214-008-9419-z

Hiro M, Sato T (1971) Infrared absorption spectra of silica gel-water, water-d_2, and water-^{18}O systems Bull Chem Soc Jpn 44:33-37

Hörst SM (2017) Titan's atmosphere and climate J Geophys Res: Planets 122:432-482 doi:10.1002/2016je005240

Huang C, Behrman EC (1991) Structure and properties of calcium aluminosilicate glasses Journal of Non-Crystalline Solids 128:310-321 doi:10.1016/0022-3093(91)90468-l

Huffman M, McMillan P (1985) Infrared and raman studies of chemically vapor deposited amorphous silica Journal of Non-Crystalline Solids 76:369-379 doi:10.1016/0022-3093(85)90011-0

Ilieva A, Mihailova B, Tsintsov Z, Petrov O (2007) Structural state of microcrystalline opals: A Raman spectroscopic study Am Mineral 92:1325-1333 doi:10.2138/am.2007.2482

Kamiya K, Oka A, Nasu H, Hashimoto T (2000) Comparative Study of Structure of Silica Gels from Different Sources J Sol-Gel Sci Technol 19:495-499 doi:10.1023/a:1008720118475

Khalil EMA, ElBatal FH, Hamdy YM, Zidan HM, Aziz MS, Abdelghany AM (2010) Infrared absorption spectra of transition metals-doped soda lime silica glasses Physica B: Condensed Matter 405:1294-1300 doi:10.1016/j.physb.2009.11.070

Kivi N, Moore A, Dyar K, Haaf S (2016) Devitrification Rates of Fused Silica in the Presence of Trace Impurities

Kochemasov G (1985) Attention: fulgurite! Lunar and Planetary Science Conference 16:443-444

Koeberl C, Ferrière L (2019) Libyan Desert Glass area in western Egypt: Shocked quartz in bedrock points to a possible deeply eroded impact structure in the region Meteoritics & Planetary Science 54:2398-2408 doi:10.1111/maps.13250

Langer K, Floerke O (1974) Near infrared absorption spectra (4000-9000 cm^{-1}) of opals and the role of "water" in these $SiO_2.nH_2O$ minerals Fortschr Miner 52:17-51

Liesegang M, Milke R (2014) Australian sedimentary opal-A and its associated minerals: Implications for natural silica sphere formation Am Mineral 99:1488-1499 doi:10.2138/am.2014.4791

Maierhofer K, Koeberl C, Brigham-Grette J (2019) Petrography and geochemistry of the impact to postimpact transition layer at the El'gygytgyn impact structure in Chukotka, Arctic Russia Meteoritics & Planetary Science 54:2510-2531 doi:10.1111/maps.13243

Martín-Ramos P, Gil FPSC, Martín-Gil FJ, Martín-Gil J (2019) Characterization of exogenic fulgurites from an archaeological site in Tiedra, Valladolid, Spain Geological Magazine:1-8 doi:10.1017/s0016756819000438

McMillan PF, Remmele RL (1986) Hydroxyl sites in SiO_2 glass: A note on infrared and Raman spectra Am Mineral 71:772-778

Moenke HHW (1974) Silica, the three-dimensional silicates, borosilicates and beryllium silicates. In: Farmer VC (ed) The Infrared Spectra of Minerals, vol 4. Mineralogical Society of Great Britain and Ireland, London, UK, pp 365-382. doi:10.1180/mono-4.16

Mohling JW (2004) Exogenic fulgurites from Elko County, Nevada: A new class of fulgurite associated with large soil-gravel fulgurite tubes Rocks Miner 79:334-340 doi:10.1080/00357529.2004.9925733

Mysen BO, Richet P (2005) Silicate glasses and melts: properties and structure. Developments in Geochemistry, vol 10, 1st edn. Elsevier, Amsterdam; Boston

Navarro-González R et al. (2007) Paleoecology reconstruction from trapped gases in a fulgurite from the late Pleistocene of the Libyan Desert Geology 35 doi:10.1130/g23246a.1

Osinski GR et al. (2008) The Dakhleh Glass: Product of an impact airburst or cratering event in the Western Desert of Egypt? Meteoritics & Planetary Science 43:2089-2107

Ostrooumov M, Fritsch E, Lefrant S (1999) Primeros datos sobre la espectrometría Raman de los ópalos Rev Mex Cienc Geol 16:4

Pasek M, Block K (2009) Lightning-induced reduction of phosphorus oxidation state Nature Geoscience 2:553-556 doi:10.1038/ngeo580

Pasek MA, Block K, Pasek V (2012) Fulgurite morphology: a classification scheme and clues to formation Contrib Mineral Petrol 164:477-492 doi:10.1007/s00410-012-0753-5

Pasek MA, Pasek VD (2018) The forensics of fulgurite formation Mineral Petrol 112:185-198 doi:10.1007/s00710-017-0527-x

Perry CC, Li X, Waters DN (1991) Structural studies of gel phases—IV. An infrared reflectance and Fourier transform Raman study of silica and silica/titania gel glasses Spectrochim Acta, Pt A: Mol Spectrosc 47:1487-1494 doi:10.1016/0584-8539(91)80240-j

Petculescu A, Kruse R (2014) Predicting the characteristics of thunder on Titan: A framework to assess the detectability of lightning by acoustic sensing J Geophys Res: Planets 119:2167-2176 doi:10.1002/2014je004663

Plyusnina II (1979) Infrared spectra of opals Sov Phys Dokl 24:332-333

Reyes-Salas AM et al. (2017) Estudio petrográfico, geoquímico y mineralógico de la fulgurita San José de Lourdes, Zacatecas, México Rev Mex Cienc Geol 34:170-181 doi:10.22201/cgeo.20072902e.2017.3.477

Roberts SE, Sheffer AA, McCanta MC, Dyar MD, Sklute EC (2019) Oxidation state of iron in fulgurites and Trinitite: Implications for redox changes during abrupt high-temperature and pressure events Geochim Cosmochim Acta 266:332-350 doi:10.1016/j.gca.2019.08.021

Russell CT, Zhang TL, Delva M, Magnes W, Strangeway RJ, Wei HY (2007) Lightning on Venus inferred from whistler-mode waves in the ionosphere Nature 450:661-662 doi:10.1038/nature05930

Sheffer AA (2007) Chemical reduction of silicates by meteorite impacts and lightning strikes. The University of Arizona

Silvia PJ The Civilization-Ending 3.7KYrBP Event: Archaeological Data, Sample Analysis, and Biblical Implications. In: 80th Annual Meeting of the Meteoritical Society, Santa Fe, New Mexico, 2017/07/1 2017. p 6001

Smallwood AG, Thomas PS, Ray AS (1997) Characterisation of sedimentary opals by Fourier transform Raman spectroscopy Spectrochimica Acta Part A: Molecular and Biomolecular Spectroscopy 53:2341-2345 doi:10.1016/s1386-1425(97)00174-1

Smith BY, Turner SJ, Rodgers KA (2018) Opal-A and associated microbes from Wairakei, New Zealand: the first 300 days Mineralogical Magazine 67:563-579 doi:10.1180/0026461036730118

Stefano CJ, Hackney SA, Kampf AR (2020) The occurrence of iron silicides in a fulgurite: Implications for fulgurite genesis The Canadian Mineralogist 58:115-123 doi:10.3749/canmin.1900019

Taylor W (1987) The petrogenetic role of methane: Effect on liquidus phase relations and the solubility mechanisms of reduced CH volatiles. In: Mysen BO (ed) Magmatic processes: physicochemical principles, vol 1. Geochemical Society Special Publications. Geochemical Society, University Park, PA, USA, pp 121-138

Templin EH, Mowery IC, Kunze GW (1956) Houston Black Clay, the Type Grumusol: I. Field Morphology and Geography Soil Sci Soc Am J 20 doi:10.2136/sssaj1956.03615995002000010022x

The University of Texas at Austin. Bureau of Economic Geology (1992) Geology of Texas.

Uchino T, Sakka T, Iwasaki M (1991) Interpretation of Hydrated States of Sodium Silicate Glasses by Infrared and Raman Analysis J Am Ceram Soc 74:306-313 doi:10.1111/j.1151-2916.1991.tb06880.x

United States Geological Survey (USGS) (2014) Geologic Database of Texas, 2014-02-01. https://data.tnris.org/collection/79a18636-3419-4e22-92a3-d40c92eced14. 2019

Walrafen GE (1964) Raman Spectral Studies of Water Structure The Journal of Chemical Physics 40:3249-3256 doi:10.1063/1.1724992

Walter M (2011) An exogenic fulgurite occurrence in Oswego, Oswego County, New York Rocks Miner 86:264-270 doi:10.1080/00357529.2010.517134

Wan W, Feng Y, Yang J, Bu W, Qiu T (2016) Microstructure, mechanical and high-temperature dielectric properties of zirconia-reinforced fused silica ceramics Ceram Int 42:6436-6443 doi:10.1016/j.ceramint.2016.01.063

Wannier MMA, de Urreiztieta M, Wenk H-R, Stan CV, Tamura N, Yue B (2019) Fallout melt debris and aerodynamically-shaped glasses in beach sands of Hiroshima Bay, Japan Anthropocene 25 doi:10.1016/j.ancene.2019.100196

Warren BE, Loring AD (1935) X-Ray Diffraction Study of the Structure of Soda-Silica Glass J Am Ceram Soc 18:269-276 doi:10.1111/j.1151-2916.1935.tb19394.x

Wasson JT (2003) Large aerial bursts: An important class of terrestrial accretionary events Astrobiology 3:163-179 doi:10.1089/153110703321632499

Webb JA, Finlayson BL (1987) Incorporation of Al, Mg, and water in opal-A; evidence from speleothems Am Mineral 72:1204-1210

White WB, Minser DG (1984) Raman spectra and structure of natural glasses Journal of Non-Crystalline Solids 67:45-59 doi:10.1016/0022-3093(84)90140-6

Winter JD (2010) Principles of igneous and metamorphic petrology. 2nd edn. Pearson, Edinburgh

FIGURE CAPTIONS

Fig 1 (a) Libyan “desert glasses” from Dakhleh Oasis and other sites in the Great Sand Sea at the Egyptian-Libyan border, originated from sand melted by a meteorite. (b) Fallout melt debris and aerodynamically-shaped glasses in beach sands of Motoujina, Hiroshima Bay, Japan, related to the nuclear explosion in 1945. Reproduced with permission from Wannier et al. (2019). (c,d) Assortment of backlit teardrops (Bunch et al. 2012) and a trinitite sample from Trinity site, Alamogordo, NM, USA, generated after the explosion of the first atomic bomb in 1945. (e) Glassy impactite with multiple accretionary nodules from Meteor Crater, near Winslow, Northern Arizona, USA (as part of the Younger Dryas cooling episode 12.9KYrBP) (Bunch et al. 2012). (f,g) Desert glass sample and glassified ceramic slag from Tall el-Hammam area, Jordan, resulting from the 3.7KYrBP Kikkar Event.

Fig 2 (a) Exogenic fulgurite from Elko Hills, Elko County, NV, USA (size: 27×19×16 mm; weight: 5.32 g) (Mohling 2004); (b) exogenic fulgurite from Oswego, Oswego County, NY, USA (Walter 2011); (c,d) droplet fulgurite with protuberances from Dallas, TX, USA. The space between two adjacent unit-and-value hatch marks in (c) represents a millimeter.

Fig 3 Left: Mesquite area geologic map (data from U.S. Geological Survey (United States Geological Survey (USGS) 2014)); right: Geology of Texas map (The University of Texas at Austin. Bureau of Economic Geology 1992).

Fig 4 Optical microphotographs (at 500× magnification) of the small spherical protuberances (1-2 mm diameter) on the surface of the droplet fulgurite: (a,b) adjacent light-halo craters on the surface of microprotuberance #1; (c) surface of microprotuberance #2; (d) nipple and scratches/stretch marks on microprotuberance #3.

Fig 5 SEM micrographs of the surface of the microprotuberances on the exogenic fulgurite specimen. Operative conditions: (a) magnification=203X, acceleration voltage=15 kV, working distance=11 mm, probe current=44 pA, stage at Z=25 mm; (b) magnification=223X, acceleration voltage=15 kV, working distance=11.6 mm, probe current=10 pA, stage at Z=25 mm; (c) magnification=207X, acceleration voltage=15 kV, working distance=10.5 mm, probe current=11 pA, stage at Z=25 mm.

Fig 6 SEM-BSE image of a spherule from Abu Hureyra (product of Younger Dryas episode 12.9KYrBP) that shows high-temperature flow lines or *schlieren* (reproduced with permission from Bunch et al. (2012))

Fig 7 X-ray powder diffraction pattern of the exogenic fulgurite from Dallas, TX, USA.

Fig 8 FTIR spectrum of the exofulgurite specimen from Dallas, TX, USA (black solid line): (a) full spectral range; (b) 1600–400 cm^{-1} region; (c) 4000-1400 cm^{-1} region. Spectra from quartz (dotted black line) and opal (dotted red line) are also shown for comparison purposes. The inset in (a) shows the bands in the 3100–2200 cm^{-1} region in higher detail.

Fig 9 Raman spectrum of the exofulgurite specimen from Dallas, TX, USA (black solid line): (a) full spectral range; (b) 100–1300 cm^{-1} region. Spectra from quartz (dotted black line) and opal (dotted red line) are also shown for comparison purposes.

TABLES

Table 1. Analysis of major and minor elements as oxides for the exogenic fulgurite sample from Dallas, TX, USA.

Oxide	**SiO_2**	**TiO_2**	**Al_2O_3**	**Fe_2O_3**	**MnO**	**MgO**	**CaO**	**Na_2O**	**K_2O**	**P_2O_5**	**ZrO_2**	**SrO**	**Y_2O_3**
XRF	62.43	0.89	11.41	8.21	0.25	0.86	14.09	0.34	1.35	0.16	-	-	-
XRF	64.83	0.58	16.30	3.70	0.14	1.15	11.78	0.36	1.09	0.02	0.047	0.026	0.012
EDX	69.72	-	18.10	-	-	1.90	8.58	-	1.69	-	-	-	-

Table 2. Bulk abundance (wt%) of major oxides in fulgurites from different origins.

Oxide	**Dallas, TX, USA**		**York, PA, USA**	**Vernal, UT, USA**	**Greensboro, NC, USA**	**Pº do Vasco, Viseu, Portugal**		**Tiedra, Valladolid, Spain**		**Mottarone, Baveno, Piedmont, Italy**		**"San José de Lourdes", Zacatecas, México**	
	Avg.	(min-max)				Avg.	(min-max)	Avg.	(min-max)	Avg.	(min-max)	core	cover
SiO_2	63.63	(62.43-64.83)	55.49	67.60	81.30	68.93	(68.13-69.72)	61.45	(59.1-63.8)	73.90	(71.97-75.79)	60.84	71.83
TiO_2	0.73	(0.58-0.89)	1.23	0.51	1.15	0.80	(0.77-0.83)	0.65	(0.5-0.8)	0.04	(0.03-0.05)	0.28	0.42
Al_2O_3	13.86	(11.41-16.30)	25.75	13.91	8.32	16.14	(15.97-16.30)	8.40	(8.1-8.7)	7.70	(7.54-7.79)	10.13	14.17
$Fe_2O_3^*$	5.95	(3.70-8.21)	6.36	3.69	8.48			10.00	(9.4-10.6)			2.47	4.04
FeO^*						3.09	(2.50-3.67)			0.38	(0.22-0.51)		
MnO	0.19	(0.14-0.25)	0.07	0.65	0.28	-		0.45	(0.4-0.5)	0.06	(0.02-0.10)	0.04	0.09
MgO	1.01	(0.86-1.15)	1.63	2.58	0.10	0.29	(0.19-0.39)	2.40	(2.0-2.8)	0.24	(0.20-0.26)	1.33	1.31
CaO	12.94	(11.78-14.09)	1.71	5.20	0.15	-		11.80	(10.5-13.1)	0.80	(0.75-0.83)	18.56	3.82
Na_2O	0.35	(0.34-0.36)	0.75	3.74	0.04	3.40	(3.39-3.40)	-	-	0.05	(0.04-0.07)	0.47	0.85
K_2O	1.22	(1.09-1.35)	4.35	2.92	0.18	7.43	(7.30-7.56)	3.90	(3.3-4.5)	0.20	(0.12-0.28)	2.80	3.35
P_2O_5	0.09	(0.02-0.16)	0.08	0.76	0.01	-		0.70	(0.5-0.9)	0.25	(0.07-0.50)	0.07	0.07
Total	99.97		97.42	101.56	100.01	100.08		99.75		83.61		96.99	99.95
Ref.	This work		(Pasek et al. 2012)		(Carter et al. 2010a)	(Abrunhosa et al. 1995)		(Martín-Ramos et al. 2019)		(Elmi et al. 2017)		(Reyes-Salas et al. 2017)	
CIPW Norm (wt %)													
q**	34.57		28.61	29.30	79.94	25.15		28.88		71.14		21.89	44.12
an	32.62		7.96	3.52	0.68					2.34		17.26	18.49
ab	2.96		6.35	31.65	1.34	23.95		11.40		0.42		3.98	7.19
or	7.21		25.71	17.26	1.06	43.85		23.05		1.18		16.55	19.80
c			16.89	3.31	7.81	2.75				6.55			2.37
di	5.70							12.90				7.15	
hy			4.06	6.43	0.25	0.82				1.34			3.26

wo	9.11					10.66		26.87	
ru		1.15		0.83	0.47				0.32
il	0.41	0.15	0.97	0.60		1.07	0.08		0.19
mt			0.64						
hm	5.95	6.36	3.25	8.48	3.09	10.00		2.47	4.04
ap	0.21	0.19	1.76	0.02		1.62	0.58	0.16	0.16
tn	1.27					0.34		0.58	

[*] Fe_2O_3(total) and FeO(total)

[**] *q, an, ab, or, c, di, hy, wo, ru, il, mt, hm, ap* and *tn* stand for quartz, anortite, albite, orthoclase, corundum, diopside, hypersthene, wollastonite, rutile, ilmenite, magnetite, hematite, apatite and titanite, respectively (Cross et al. 1912). Cells highlighted in green and yellow indicate fulgurites belonging to the normative corundum + hypersthene group and to the diopside + wollastonite + titanite group, respectively.

Table 3. Main bands in FTIR and Raman spectra (in cm^{-1}) and their assignments for the exogenic fulgurite sample from Dallas, together with some proxies used for comparison purposes.

Spectroscopic technique	Fulgurite	Opal-A*	Pure silica glass	Calcium aluminosilicate glass	Assignment
FTIR		3640–3650			Isolated silanol group vibrations
	3400	3410/3421			ν_{as}(O–H), H-bound Si–OH
		3230-3250			Stretching modes of liquid water (physisorbed H_2O)
	2961 (w)				ν_{as}(C–H) of $-CH_3$
	2926 (w)				ν_{as}(C–H) of $>CH_2$
	2855 (w)				ν_s(C–H) of $>CH_2$
	2358 (w)				δ(Al–OH)+ν(O–H) / ν(O=C=O), CO_2
	2000	1996/2007			H_2O, OH^- overtone vibration
	1880	1880/1883			
	1631	1631/1636			δ(H–O–H)
	1175				ν(Si–O)
	1069	1061	1110	1065	ν_{as}(Si–O)
	965	965		960	ν(Si–O), isolated Si–OH and/or (Si(OA1/Ca)$_2$
	784	793	805	780	ν_s(Si–O)
	460	453	452–468	464	δ(O–Si–O)
Raman	235				
	480	463.5			τ(Si–O–Si) and δ(Si–O–Si)
	800				ν_s(Si–O), silica tetrahedra
	1014	962 1066			
	2060				
	3080				ν(O–H), molecular H_2O groups

* (Adamo et al. 2010; Aines and Rossman 1984; Eckert et al. 2015; Gemological Institute of America 2020; Ilieva et al. 2007; Langer and Floerke 1974)

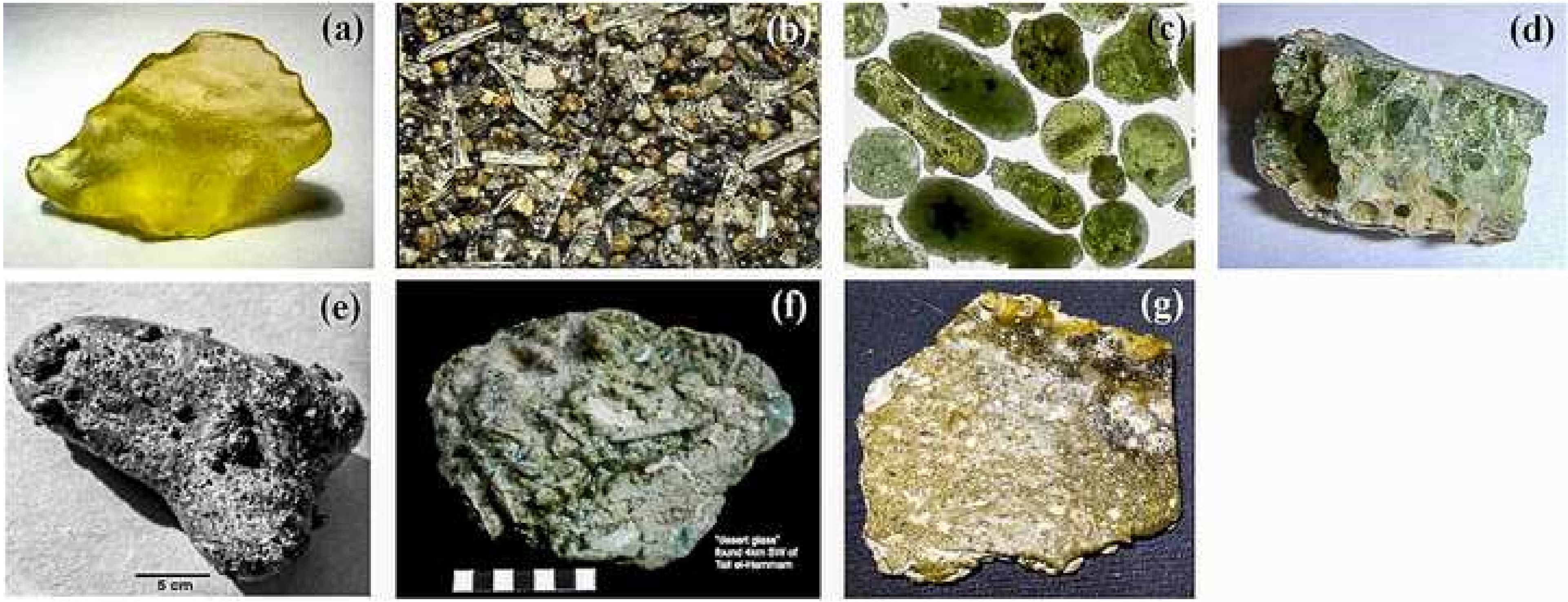
(a)
(b)
(c)
(d)
(e)
5 cm
(f)
(g)

Fig2

Click here to access/download;Figure;Fig2.jpg

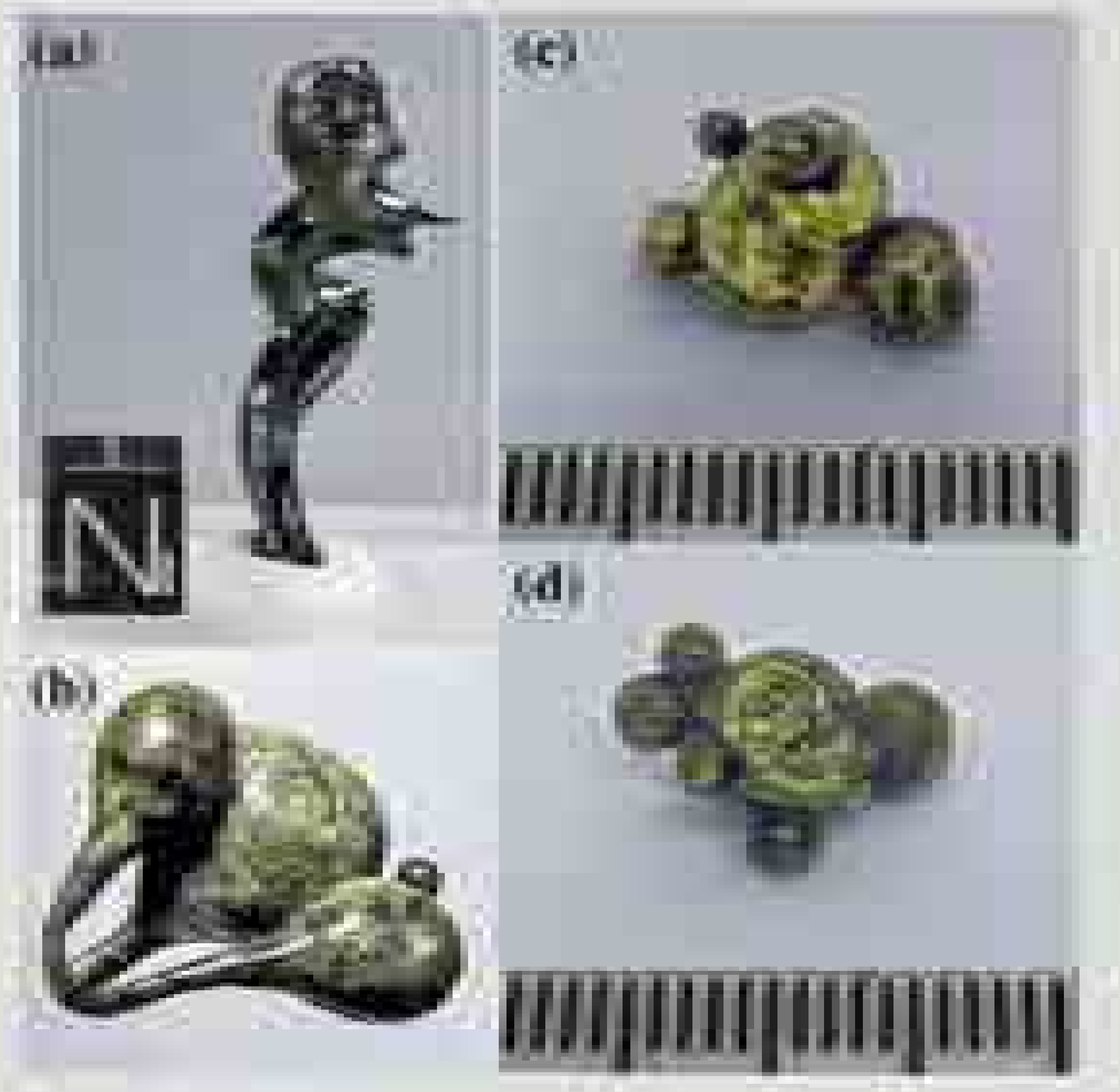

Fig3

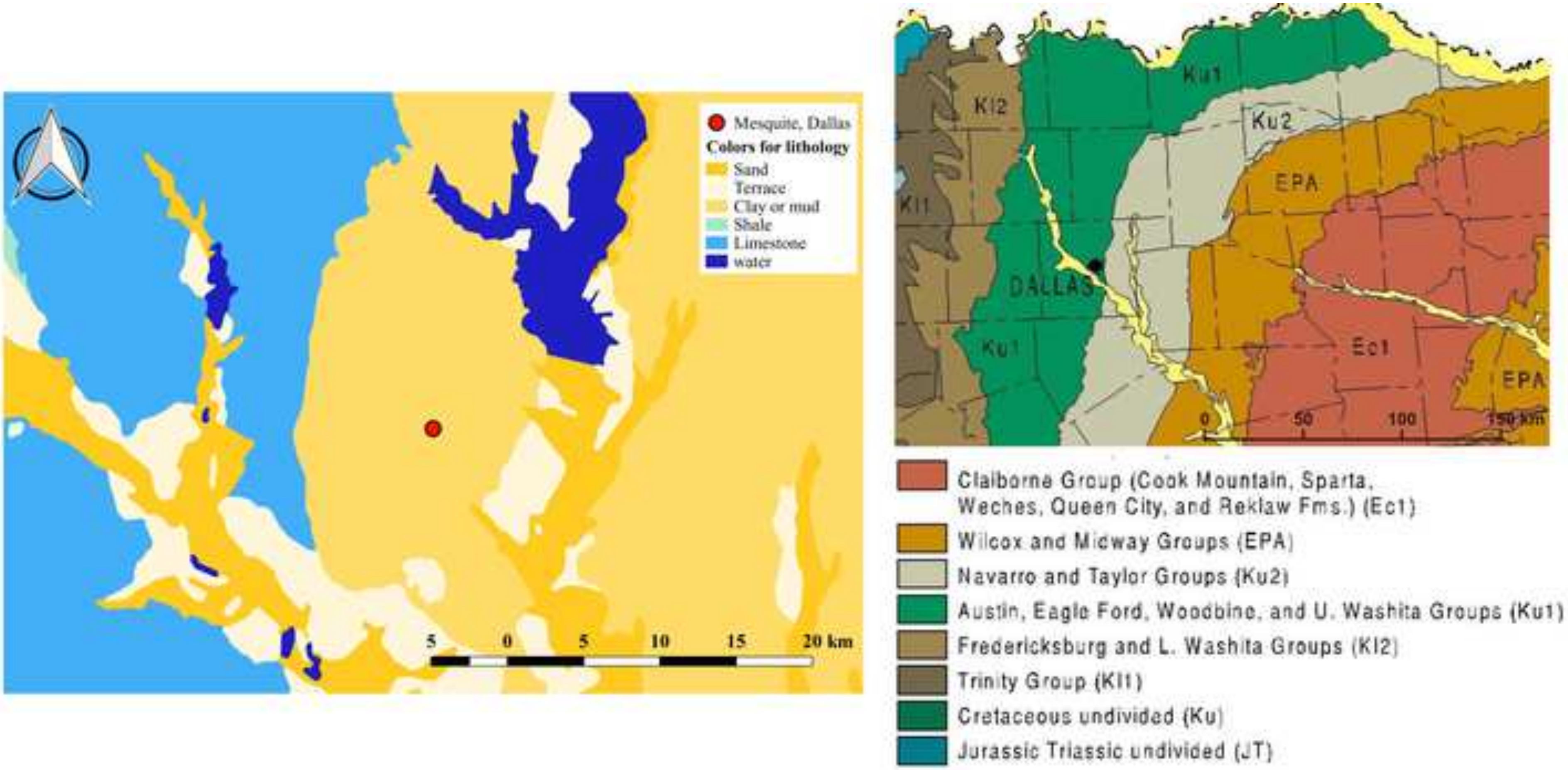
Mesquite, Dallas
Colors for lithology
Sand
Terrace
Clay or mud
Shale
Limestone
water
5 0 5 10 15 20 km
Ku1
Kl2
Ku2
EPA
Kl1
DALLAS
Ku1
Ec1
EPA
0 50 100 150 km
Claiborne Group (Cook Mountain, Sparta, Weches, Queen City, and Reklaw Fms.) (Ec1)
Wilcox and Midway Groups (EPA)
Navarro and Taylor Groups (Ku2)
Austin, Eagle Ford, Woodbine, and U. Washita Groups (Ku1)
Fredericksburg and L. Washita Groups (Kl2)
Trinity Group (Kl1)
Cretaceous undivided (Ku)
Jurassic Triassic undivided (JT)

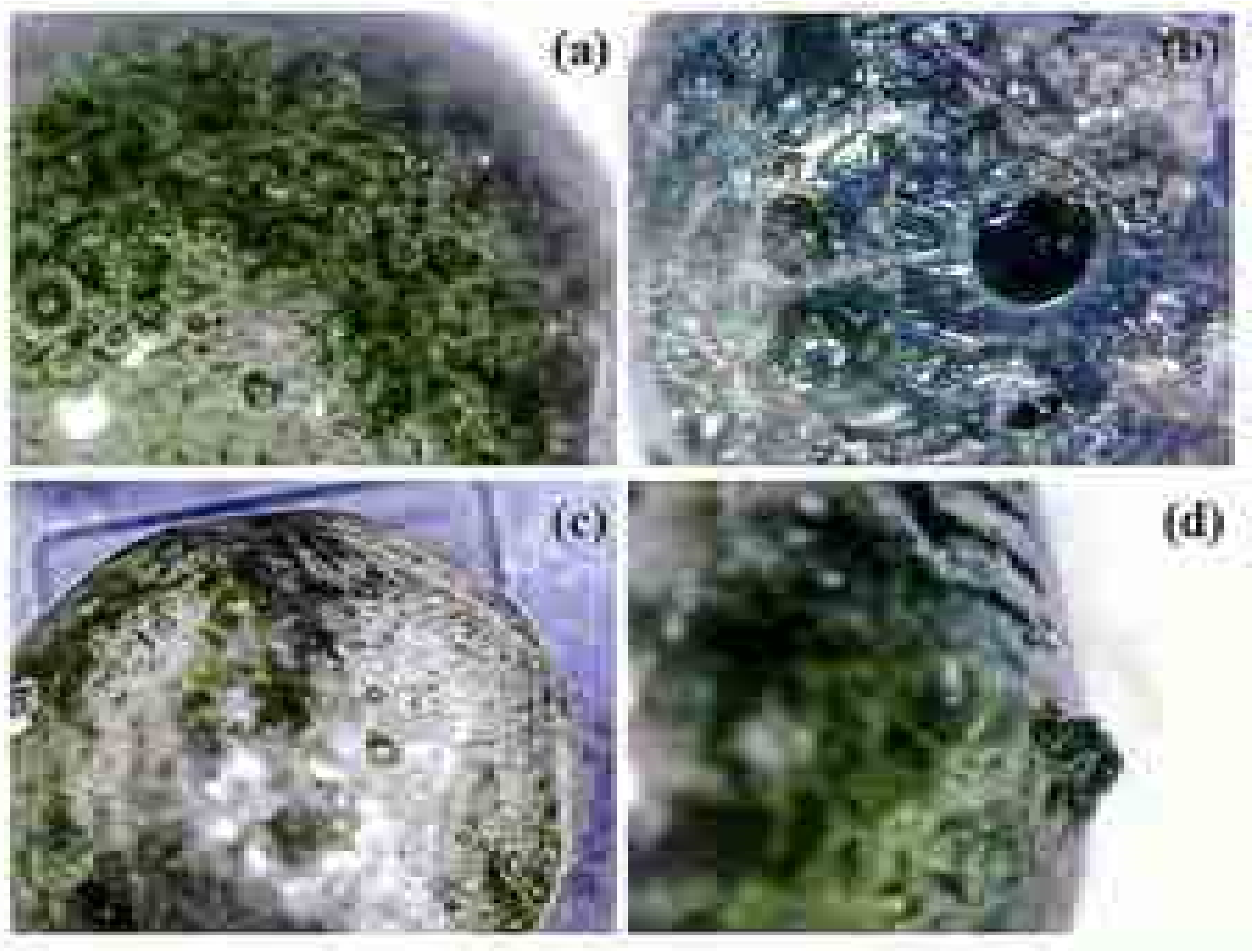
(a)
(b)
(c)
(d)

Fig5

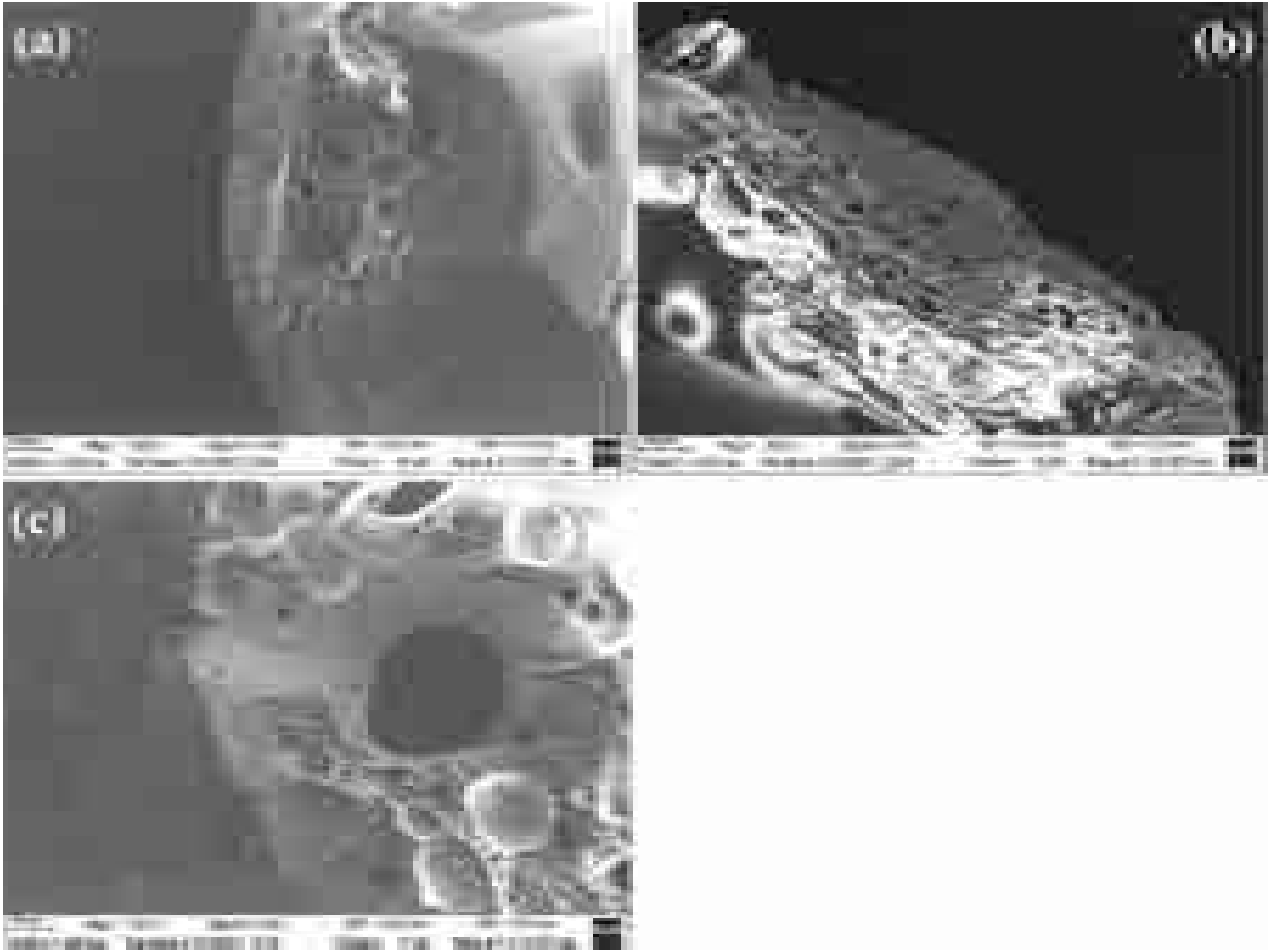

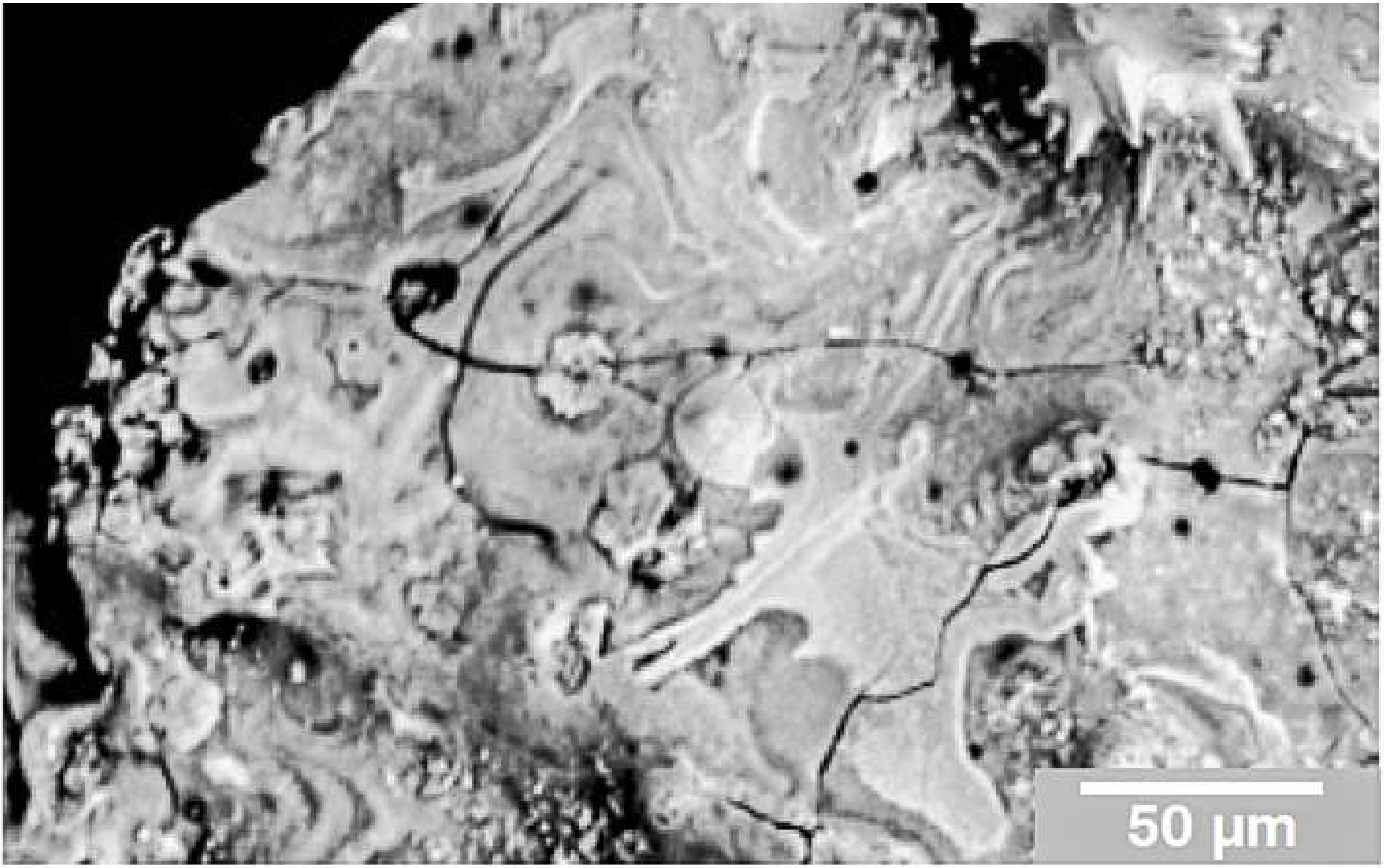
50 µm

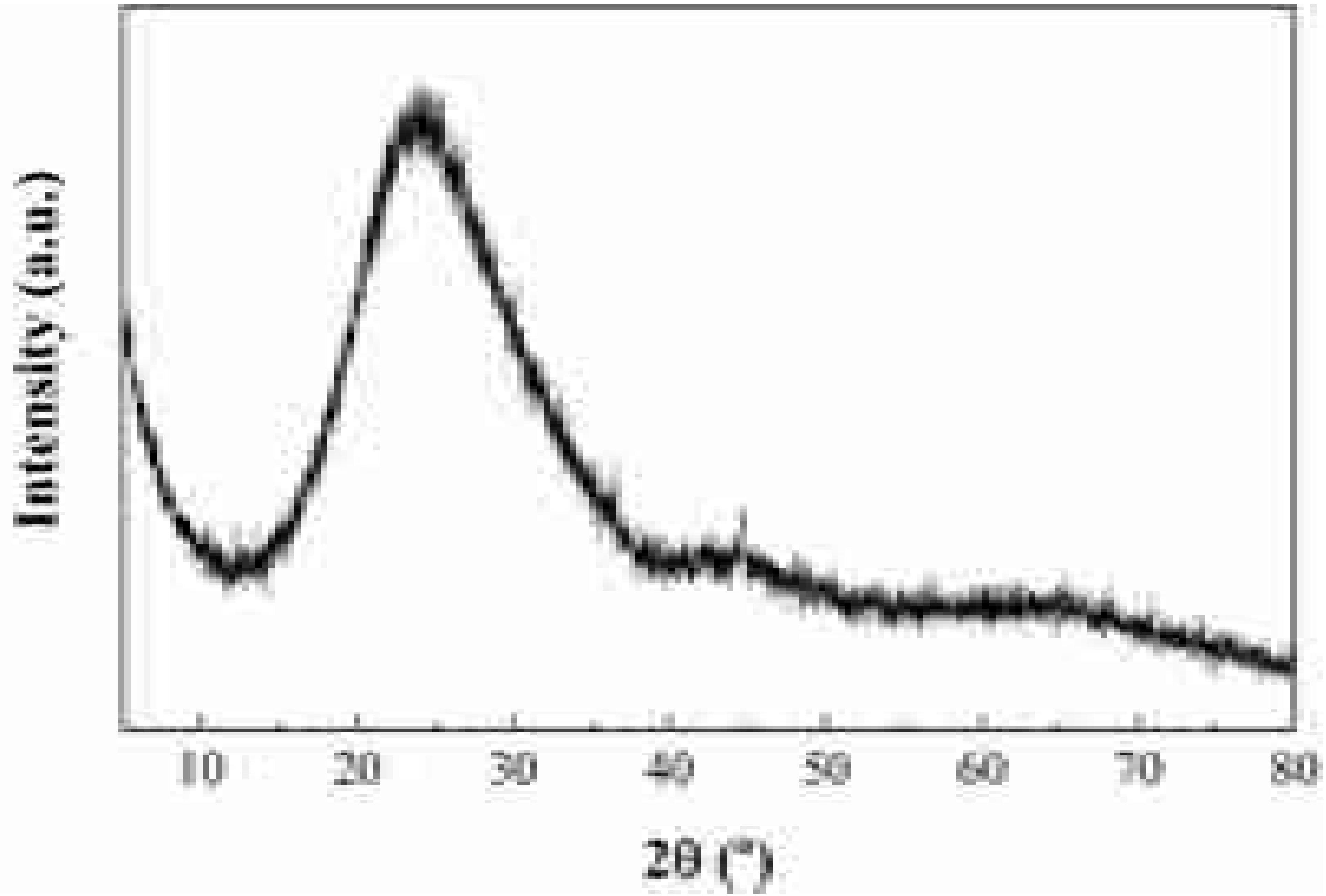
Intensity (a.u.)
10
20
30
40
50
60
70
80
2θ (°)

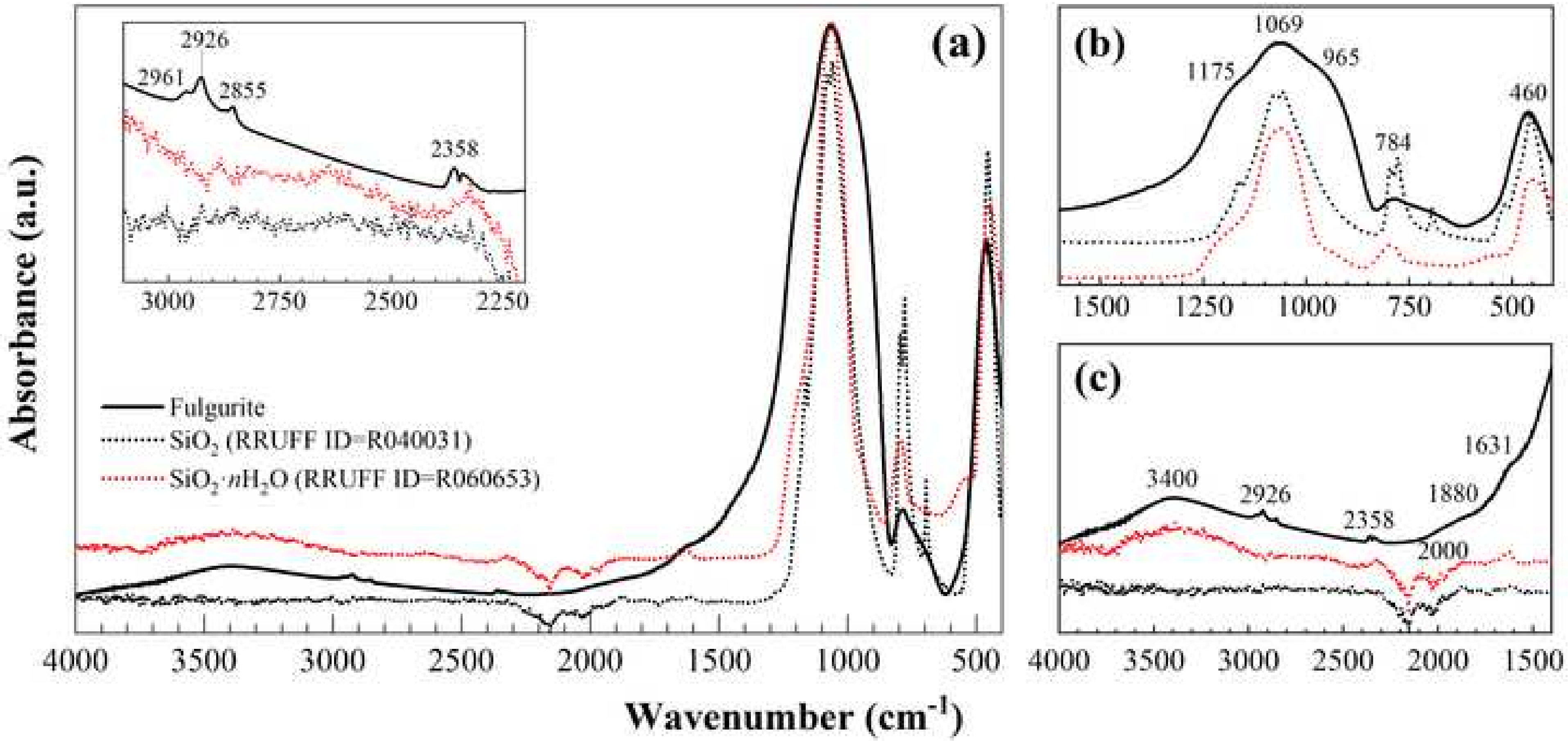
(a)
(b)
(c)
Absorbance (a.u.)
Wavenumber (cm^{-1})
Fulgurite
SiO$_2$ (RRUFF ID=R040031)
SiO$_2$·nH$_2$O (RRUFF ID=R060653)
2926
2961
2855
2358
3000
2750
2500
2250
4000
3500
3000
2500
2000
1500
1000
500
1069
1175
965
784
460
1500
1250
1000
750
500
3400
2926
2358
1631
1880
2000
4000
3500
3000
2500
2000
1500

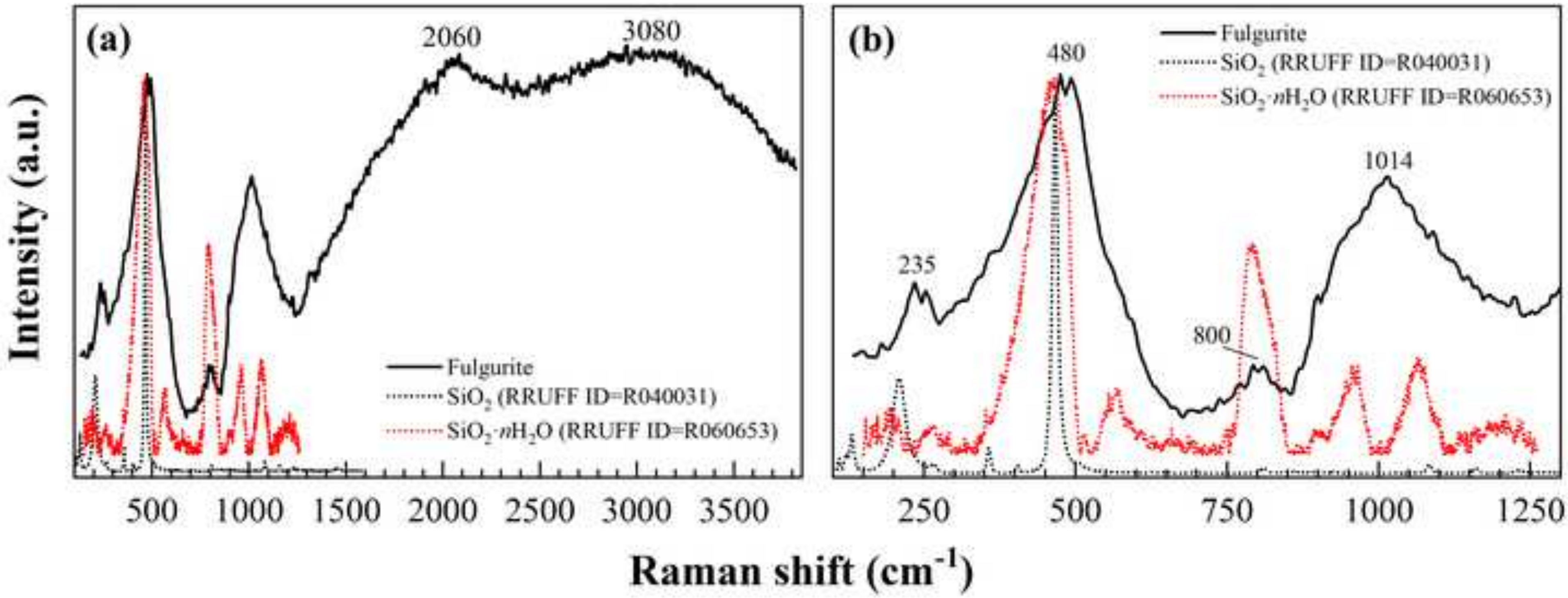
(a)
2060
3080
Fulgurite
SiO$_2$ (RRUFF ID=R040031)
SiO$_2$·nH$_2$O (RRUFF ID=R060653)
500
1000
1500
2000
2500
3000
3500
(b)
480
235
800
1014
Fulgurite
SiO$_2$ (RRUFF ID=R040031)
SiO$_2$·nH$_2$O (RRUFF ID=R060653)
250
500
750
1000
1250
Intensity (a.u.)
Raman shift (cm^{-1})